DOI:
10.1242/jcs.223974

Document Version
Peer reviewed version

Heterotypic contact inhibition of locomotion can drive cell sorting between epithelial and mesenchymal cell populations

Simon Brayford[1], Fiona N. Kenny[1], Toru Hiratsuka[2], Eduardo Serna-Morales[1], Lawrence Yolland[1], Andrei Luchici[3], and Brian M. Stramer[1]*

[1] Randall Centre for Cell and Molecular Biophysics, King's College London, SE1 1UL, London, United Kingdom

[2] Centre for Stem Cells and Regenerative Medicine, King's College London, SE1 9RT, London, United Kingdom

[3] Dacian Consulting, 84 Brookwood Road, SW18 5BY, London, United Kingdom

* Correspondence: brian.m.stramer@kcl.ac.uk

ABSTRACT

Interactions between different cell-types can induce distinct contact inhibition of locomotion (CIL) responses that are hypothesised to control population-wide behaviours during embryogenesis. However, our understanding of the signals that lead to cell-type specific repulsion and the precise capacity of heterotypic CIL responses to drive emergent behaviours is lacking. Using a new model of heterotypic CIL, we show that fibrosarcoma cells, but not fibroblasts, are actively repelled by epithelial cells in culture. We show that knocking down EphB2 or ERK in fibrosarcoma cells specifically leads to disruption of the repulsion phase of CIL in response to interactions with epithelial cells. We also examine the population-wide effects when these various cell combinations are allowed to interact in culture. Unlike fibroblasts, fibrosarcoma cells completely segregate from epithelial cells and inhibiting their distinct CIL response by knocking down EphB2 or ERK also disrupts this emergent sorting behaviour. These data suggest that heterotypic CIL responses, in conjunction with processes such as differential adhesion, may aid the sorting of cell populations.

INTRODUCTION

Contact inhibition of locomotion (CIL) is a process whereby a cell ceases motility or changes trajectory upon collision with another cell. The response can occur between cells of the same type (homotypic) or between different types (heterotypic) leading to distinct dynamics depending on the cell-type and the receptors expressed on their surface (Stramer and Mayor, 2016).

Our understanding of the functional significance of CIL for animal physiology is only beginning to be elucidated. Differential homotypic and heterotypic CIL dynamics have recently been shown to play a role in animal development (Theveneau et al., 2013) and a loss of heterotypic CIL is hypothesised to play a role in cancer metastasis (Abercrombie, 1979), yet the signals behind these responses are only starting to emerge. In this study, through screening cell-types for distinct CIL behaviours we report that fibrosarcoma cells, rather than losing their heterotypic CIL response after contact with epithelial cells as previously predicted (Abercrombie, 1979), are actively repelled via an Eph/ERK signalling cascade, highlighting that not all cancer cells are necessarily CIL deficient. Interestingly, when fibrosarcoma and epithelial cells are allowed to mix in culture, the heterotypic repulsion between them leads to sorting and segregation of the populations. Recent work suggested that differential adhesion, the predominant mechanism hypothesised to drive cell sorting, is inadequate in predicting the segregation of mesenchymal populations (Pawlizak et al., 2015, Tambe and Fredberg, 2015) and our data suggest that CIL may be an additional mechanism behind this important developmental phenomenon.

RESULTS AND DISCUSSION

Fibroblasts and fibrosarcoma cells exhibit distinct responses upon collision with epithelial cells

To study heterotypic cell-cell collisions, we used a confrontation assay whereby two different cell populations were allowed to migrate and collide. Following a screen of different epithelial versus mesenchymal cell-types, an unexpected phenomenon was revealed. When migrating epithelial cells (HaCaT) encountered migrating fibroblasts (NIH3T3), both populations ceased their forward motion, forming a sharp border (Fig. 1A and Movie 1). In contrast, fibrosarcoma cells (HT1080) seemed to undergo repulsion following collision with epithelial cells (Fig. 1A,B and Movie 1). Interestingly, this repulsive response was not observed with melanoma cell-lines (Fig.

S1A,B and Movie 2), suggesting that fibrosarcoma cells may have an enhanced heterotypic CIL response.

When no colliding partner was encountered, HaCaT cells migrated with a constantly increasing speed (Fig. 1C), which was also observed following their collision with HT1080 cells (Fig. 1D), suggesting that epithelial migration was unaffected by collision with the HT1080 population. In contrast, HaCaT migration was severely reduced following collision with fibroblasts (Fig. 1D). The repulsion of fibrosarcoma cells was further analysed using particle image velocimetry, which revealed a population-wide increase in epithelial cell speed following collision with fibrosarcoma cells (Fig. 1E and Movie 3) showing that fibrosarcoma cells have a distinct response to epithelial cells.

Fibrosarcoma cells undergo active repulsion from epithelial cells

To determine whether fibrosarcoma cell repulsion by epithelial cells was an active process, we examined individual cell collisions (Movie 4). Analysis of acceleration changes before and after collisions revealed that when fibrosarcoma cells collided with epithelial cells there was a rapid, rearward acceleration (Fig. 2A) suggesting a sudden change in motion. This response was similar to previously reported collisions between *Drosophila* macrophages, which also undergo a classical CIL response involving active repulsion (Davis et al., 2012, Davis et al., 2015). The backward acceleration of fibrosarcoma cells was accompanied by a shift in the direction of their velocities before, during, and after the collision as fibrosarcoma cells were repelled from epithelial cells (Fig. 2B). In contrast, repulsion was not observed when fibroblasts collided with epithelial cells, nor during homotypic fibrosarcoma collisions, where cells continued to migrate toward the colliding partner after collision (Fig. 2A and B). Plotting the distance from collision over time revealed that heterotypic collisions led to fibrosarcoma cells slowing before migrating away from epithelial cells, in contrast to homotypic collisions, which led to their continued forward motion (Fig. 2C). These data highlight that fibrosarcoma cells show distinct CIL dynamics involving active repulsion in response to collision with epithelial cells.

ERK activation downstream of EphB2 induces heterotypic repulsion of fibrosarcoma cells

There is much evidence for Eph receptors playing a role in epithelial cell

repulsion and cell segregation (Porazinski et al., 2016, Poliakov et al., 2008). However, less is known about whether ephrin signalling may control the repulsion and segregation of mesenchymal cell populations. HT1080 fibrosarcoma cells express the ephrin receptor EphB2 (Fig. S2A), knockdown of which abolished the backward acceleration upon collision with epithelial cells (Fig. 2A). This led to a random distribution of cell velocities after collision (Fig. 2B) suggesting that cells were randomly migrating away from epithelial cells rather than being actively repelled. Similarly, plotting the distance from collision over time revealed that EphB2 knockdown in fibrosarcoma cells slowed their separation from epithelial cells, further showing that the repulsion phase of CIL was disrupted (Fig. 2D). We also tested the effect of knocking down EphB2 in the confrontation assay and found that indeed, collective repulsion of fibrosarcoma cells following collision with a monolayer of epithelial cells was also impaired (Fig. S2C,D).

One signalling pathway previously reported to be controlled by Eph receptor activation is the ERK pathway. However, there is conflicting evidence for ERK signalling specifically downstream of Eph receptor activation, with some reports suggesting inhibition (Miao et al., 2003, Elowe et al., 2001) and others reporting an increase following Eph receptor stimulation (Pratt and Kinch, 2002, Vindis et al., 2003, Kandouz et al., 2010). We found that knockdown of ERK1/2 in fibrosarcoma cells phenocopied EphB2 knockdown both in single-cell collisions (Fig. 2A,B,D) and in confrontation assays (Fig. S2C,D). To confirm that these effects were related to collisions and not general migration defects we examined non-colliding fibrosarcoma cells and found no significant difference in either speed (Fig. S2E) or persistence (Fig. S2F) following EphB2 or ERK knockdown.

We also examined the temporal relationship between protrusion/retraction events surrounding collisions. We found that both EphB2 and ERK1/2 knockdown in fibrosarcoma cells led to a delay in leading-edge retraction following contact with epithelial cells (Fig. 2E). This was accompanied by a disruption to the protrusion/retraction sequence where, unlike control cells which retracted their leading-edge before forming a new protrusion, both EphB2 and ERK knockdown cells often formed a new protrusion prior to leading-edge retraction (Fig. 2F) suggesting a loss of coordinated retraction and repolarisation of lamellae after collision. Interestingly, ERK was recently shown to regulate various cytoskeletal and migratory behaviours (Yang et al., 2018, Mendoza et al., 2011, Aoki et al., 2017) and we

hypothesise that ERK is a good candidate to modulate distinct CIL dynamics.

To examine ERK activity during heterotypic interactions, we used western blotting to probe lysates from co-cultures for pERK and found that pERK was elevated among epithelial-fibrosarcoma co-cultures compared with either of these cell-types individually (Fig. 3A) suggesting that ERK activity increased when these cell-types interacted. We also found that EphB2 knockdown in fibrosarcoma cells, whilst not affecting total ERK levels (Fig. 3B), resulted in a significant decrease in pERK in epithelial-fibrosarcoma co-cultures (Fig. 3C), suggesting that ERK activation is downstream of EphB2 in the fibrosarcoma population.

To analyse ERK activation dynamics during individual cell-cell interactions, we used a FRET biosensor which has previously been demonstrated to report ERK activity in living cells (Komatsu et al., 2011). Using cells expressing the biosensor, we found in confrontation assays that ERK activity increased in fibrosarcoma cells at the migrating front after colliding with epithelial cells (Fig. 3D,E and Movie 5), but not in fibroblasts after colliding with epithelial cells (Figs. 3F and S3). We also examined co-cultures of fibrosarcoma and epithelial cells and found higher ERK activity among fibrosarcoma cells in the presence of epithelial cells compared to fibrosarcoma cells alone (Fig. 3G). Finally, we found that cells in the mixed group had a higher fluctuation in their ERK activity over time by measuring variance in ERK activity compared to fibrosarcoma only (Fig. 3H), and we hypothesise that this was due to fibrosarcoma cells constantly undergoing heterotypic collisions throughout the course of the assay. Taken together, these data suggest that ERK signalling acts downstream of EphB2 and is involved in the repulsion of fibrosarcoma cells upon their contact with epithelial cells.

Fibrosarcoma and epithelial cell populations sort in culture through CIL interactions

To examine how heterotypic CIL affects population dynamics, we generated time-lapse movies of co-cultures, and found that epithelial cells and fibroblasts formed a homogenous, interspersed population, in contrast to epithelial and fibrosarcoma cells, which immediately began to sort from one another (Fig. 4A and Movie 6). In addition, automated tracking of the mesenchymal cells in these movies revealed a streaming-type behaviour specifically among fibrosarcoma cells (Fig. 4B and Movie

6), highlighting this population's coordinated segregation from epithelial cells over time.

To examine whether the specific repulsive CIL dynamics of fibrosarcoma cells in response to epithelial cells was driving their segregation we inhibited Eph or ERK signalling in the fibrosarcoma population. Indeed, knockdown of EphB2 or ERK1/2 in fibrosarcoma cells resulted in a disruption to their segregation from epithelial cells (Fig. 4C,D). Similarly, treatment with U0126 also resulted in disruption to the segregation between fibrosarcoma and epithelial cells (Fig. S4A-C). These data suggest that segregation of fibrosarcoma from epithelial cells is driven by active repulsion between these two populations.

We also investigated the phenomenon of cell-sorting over a longer period to examine the final patterns of the populations (Fig. 4E). Alone, epithelial cells grew in clusters that eventually merged to form large colonies. However, the presence of fibroblasts resulted in much smaller clusters as the two cell populations reached equilibrium. In contrast, when grown together with fibrosarcoma cells, which proliferate at a similar rate to fibroblasts (Fig. S4D), epithelial cells formed large colonies unimpeded by the presence of fibrosarcoma cells (Fig. 4E). Furthermore, epithelial cell proliferation was specifically reduced in the presence of fibroblasts (Fig. 4F) suggesting they may undergo contact inhibition of proliferation in the absence of a repulsive heterotypic CIL response. Finally, we measured the size of individual epithelial cells and found that those in contact with fibroblasts failed to spread compared with those in contact with fibrosarcoma cells (Figs 4G and S4E). These data suggest that the repulsion of fibrosarcoma cells allows the epithelial cells to spread which may enable their proliferation, similar to other epithelial cell-types (Gumbiner and Kim, 2014, Aragona et al., 2013).

The differential adhesion hypothesis (DAH) states that two different cell-types can segregate simply by taking into account their differential adhesion and surface tension (Foty and Steinberg, 2013). This has been the predominant model to explain cell-sorting and assumes that cells segregate in a liquid-like phase separation. The problem with this concept is that groups of cells do not behave like perfect liquids; cell clusters can quickly go from a fluid-like to a solid-like state as cell density increases in a process termed 'jamming', which leads to cells rapidly slowing their motion (Sadati et al., 2013). Furthermore, the DAH has recently been found inadequate in predicting the sorting of mesenchymal cells (Pawlizak et al., 2015, Tambe and Fredberg, 2015).

Here we show that a mesenchymal cell-type can rapidly segregate from an epithelial population. Differential adhesion is still playing a role in this case due to the high surface-tension of the epithelial population and the near-non-existent mutual adhesion of the fibrosarcoma cells, leading to the less cohesive cell (HT1080) surrounding the more cohesive cell-type (HaCaT) as expected by DAH (Foty and Steinberg, 2013). However, DAH is insufficient on its own, as inhibiting heterotypic repulsion prevents sorting. We hypothesise that CIL between fibrosarcoma and epithelial cells helps fluidise the population, allowing cells to sample their adhesive landscape. Furthermore, there appears to be an aspect of fibrosarcoma CIL relieving contact inhibition of proliferation of epithelial cells, allowing epithelial colonies to grow and merge (Fig. S5). It is therefore possible that we are also highlighting an unexplored connection between CIL and contact inhibition of proliferation despite these processes being thought of as distinct behaviours (Stramer and Mayor, 2016).

It was previously hypothesised that one hallmark of cancer cells is a loss of CIL in response to neighbouring cells, which may aid their metastatic spread. However, here we reveal that not all cancer cells are deficient in heterotypic CIL; indeed, fibrosarcoma cells show a robust repulsive CIL response after contact with epithelial cells. One question is whether such a response is physiologically relevant. It is possible that both positive and negative CIL behaviours of some cancer cells observed *in vitro* may be related to an ontogenetic theory of cancer dissemination; it was recently hypothesised that some cancers may spread through permissive compartments that are defined embryologically (Hockel, 2012, Hockel, 2015) and it will be interesting to determine whether differential CIL dynamics may be playing a role in the compartmentalised spreading of metastatic cells in vivo.

MATERIALS AND METHODS

Cell culture

Cell-lines were a gift from Vicky Sanz-Moreno and Matthias Krause and were routinely tested and found to be free from mycoplasma contamination. Cells were maintained in DMEM (Sigma, St. Louis, MI cat# 6429) supplemented with 10 % FBS, at 37° C and 5 % CO_2. For routine maintenance, cells were cultured in T75 plastic cell culture flasks and split via trypsinisation approximately every 3 days or when approaching confluence.

Cell labelling

CellTracker Green CMFDA and CellTracker Red CMTPX dyes (Invitrogen, Carlsbad, CA) were used to differentially label cell-types in co-culture assays. Cells were exposed to either dye at 1 μM in serum-free medium for 30 mins at 37° C before being washed once with PBS, trypsinised and re-suspended in complete medium.

Imaging

Movies and still images were acquired using an LSM 880 inverted confocal microscope (Zeiss, Oberkochen, Germany). Cells were maintained at 37° C and 5 % CO_2 for the duration of live imaging. Images were acquired using differential interference contrast (DIC) imaging along with airyscan filter sets for 488 or 561 lasers with either a 20X (NA 0.45) air objective (Zeiss).

Confrontation assay

2-well culture inserts (Ibidi, Germany) were placed into the centre of the well of a 24 well μ-Plate (Ibidi, Germany). Two different pre-labelled cell-types were seeded into opposite chambers at a density of 1 x 10^5 cells / cm^2 and incubated overnight. The culture insert was then removed and the well topped up with 1 mL culture medium before live imaging of the resulting 500 μm gap.

Particle image velocimetry (PIV)

Time-lapse images were manually segmented prior to analysis and pseudo-speckle analysis was performed as described previously (Betz et al., 2009). The size of the search image was chosen such that it spanned the maximum expected displacement of the cells during the acquisition time. To cover the whole search image, a cross-correlation coefficient was computed between source image and a sub-image of the search image shifted by one pixel. Finally, a spatial convolution with a Gaussian kernel and temporal convolution were used to interpolate the measured displacements to cover all the pixels within the frame. The complete algorithm for this analysis, including the filtering and interpolation was implemented in MATLAB (MathWorks®, Natick, MA).

Individual cell collisions and manual tracking

Analysis of single-cell collisions was carried out by combining cells pre-labelled with Cell-Tracker Dyes (Invitrogen) at low density, plating sparsely and allowing to adhere 4 h before imaging every 1 min. For the kinematics analysis, a collision was defined as the timepoint the cell in question contacts any part of the colliding partner. The cell nucleus, which could be identified from DIC movies was manually tracked using the mTrackJ plugin for ImageJ (NIH) to calculate the x,y coordinates of the cell at all time-

252 points.

253 **Kinematics analysis**

254 Kinematics analysis of the velocity and acceleration of cells was calculated as
255 previously described (Dunn and Paddock, 1982, Davis et al., 2015). In order to assess
256 the statistical significance of the direction of cells after collision, a binomial test with a
257 probability of success of 95% was performed on the cell velocity unit vectors every
258 five minutes from 5 min before to 20 min after collision. To assess the statistical
259 significance of acceleration, a one-sample t-test of the horizontal component of the
260 vectors was performed.

261 **Gene silencing by small interfering RNA (siRNA)**

262 HT1080 cells were plated onto 6-well plates at 2 x 10^5 cells / well and allowed to attach
263 overnight. Cells were transfected with pre-validated siRNA sequences to knockdown
264 human EphB2 (Sigma, cat. no. EHU060511) or human p44/42 MAPK (ERK1/2) (Cell
265 Signalling Technologies, Cat no. 6560). Unless otherwise stated in the figure legends,
266 AllStars Negative Control siRNA (Qiagen, Venlo, Netherlands) was used as a
267 negative control. siRNA was transfected using Lipofectamine RNAiMAX reagent
268 (Invitrogen, Carlsbad, CA) according to the manufacturer's instructions. Experiments
269 were carried out 48 h post-transfection.

270 **Western blotting and antibodies**

271 Total cellular proteins from individual cells or co-cultured populations were prepared
272 by rinsing cells with cold PBS and scraping with RIPA buffer (20 mM Tris pH 7.4, 150
273 mM sodium chloride, 1% (v/v) Nonidet P-40, 0.5% (w/v) sodium deoxycholate, 1 mM
274 EDTA, 0.1% (w/v) SDS) in the presence of protease and phosphatase inhibitor
275 cocktails (Roche Diagnostics, Indianapolis, IN). 20 µg of protein per well was resolved
276 on 12.5% SDS-PAGE gels before electro-transfer to PVDF membranes. Following
277 blocking in 5% (w/v) BSA in TBST, immunoblotting was performed using anti-EphB2
278 (Cell Signalling Technology, Danvers, MA, cat. #83029), anti-GADPH (Millipore,
279 Burlington, MA, cat. #ABS16), anti-p44/42 MAPK (Cell Signalling #9102), anti-cofilin
280 (CST #5175) or anti-Phospho-p44/42 MAPK (Cell Signalling #9101) antibodies at 1 in
281 1000 dilution to detect EphB2, GAPDH, ERK1/2, cofilin and pERK1/2 (Thr202/Tyr204)
282 protein respectively. Membranes were then washed with TBST and incubated with
283 species appropriate HRP-conjugated IgG secondary antibodies (Dako, Agilent
284 Technologies, Santa Clara, CA) at 1 in 10,000. Chemiluminescence was measured
285 using ImageJ (NIH, Bethesda, MD) after applying Clarity™ Western ECL substrate

(BioRad, Hercules, CA).

FRET biosensor plasmid and Lentiviral transduction

The lentiviral plasmid of nucleus-localised FRET biosensor for ERK (EKAREV-NLS) has been previously characterised (Komatsu et al., 2011) and was a kind gift from Michiyuki Matsuda at Kyoto University, Japan. EKAREV-NLS ERK biosensor was expressed in HT1080 cells by lentiviral transduction. EKAREV-ELS in replication-defective, self-inactivating lentiviral pCSII vector was co-transfected with packaging plasmid (pCAG-HIVgp) and VSV-G-/Rev-expressing plasmid (pCMV-VSVG-RSV-Rev) into Lenti-X 293T cells (Clontech, Mountain View, CA). High-titre viral solution was prepared and used for transduction into cells. NIH3T3 cells were transfected with a pPBbsr-EKAREV-NLS plasmid encoding EKAREV-NLS in pPB piggyback backbone using jetPRIME reagent (Polyplus Transfection SA, Illkirch, France) following the manufacturer's instructions.

FRET Imaging

FRET images were obtained following methods previously reported (Aoki and Matsuda, 2009). Cells were imaged with an LSM 880 inverted confocal microscope (Zeiss, Oberkochen, Germany) using a 40X (NA 0.95) oil objective (Zeiss). Donor fluorescence protein was excited with a 458 nm laser to obtain donor and FRET signal by detection filters 483/32 and 542/27, respectively. ERK activity was determined by ratiometry (FRET/CFP) as validated previously (Aoki and Matsuda, 2009, Komatsu et al., 2011). Pseudocolour images of ERK activity (Fig. 3D) were shown in intensity modulated display (IMD). Confrontation assay FRET measurements were taken 30 mins before or 30 mins after the frame at which cell-cell collision occurred.

Short-term co-culture assays

Cells were pre-labelled with either cell-tracker red or green, counted and combined in 1:1 suspension so that 5×10^4 of each cell-type was seeded per well in a 24-well imaging μ-Plate (total of 1×10^5 cells / well). For Wild-Type assays, cells were allowed 6 h to adhere before being imaged overnight for a total of 22 h. For RNAi experiments, cells were transfected with siRNA for 48 h before being differentially labelled, combined allowed to mix for 24 h before fixation with 4% paraformaldehyde in PBS. All nuclei were then labelled with DRAQ5 (Invitrogen) before coverslips were mounted. Still Images were then acquired, and the green channel was used to create a mask over the HT1080 cells' nuclei, leaving only the HaCaT cells' nuclei visible for segmentation. Nearest neighbour distances were then calculated in ImageJ (NIH). For

U0126 MEK inhibition movies, cells were differentially labelled before being combined and allowed to adhere for 6 h. U0126 (Sigma) was then added at a concentration of 20μM to inhibit MEK/ERK signalling alongside DMSO as vehicle control, and live imaging was then commenced immediately for a total of 24 h. For quantitative analysis, HaCaT cells at 6 h and 24 h were manually segmented and nearest-neighbour distances were calculated in ImageJ (NIH).

Automated cell tracking

For automated tracking, the image channel corresponding to NIH3T3 or HT1080 cells was thresholded in ImageJ so that individual cells could be detected as particles in the TrackMate plugin and tracks generated for all cells.

Long-term co-culture assay

HaCaT cells were pelleted by centrifugation and re-suspended in CellTrace™ CFSE (Invitrogen) at a working concentration of 5 μM in PBS and incubated for 20 minutes at 37°C. Cells were again pelleted and re-suspended in fresh culture medium to a density of 2 x 10^4 cells / mL and incubated for 10 minutes to allow the CFSE reagent to undergo acetate hydrolysis. This suspension was then combined with either DMEM (control), an NIH3T3 cell suspension (unlabelled) or HT1080 cell suspension (unlabelled) and added to a 24-well plate for a total of 20,000 cells per well and incubated for 4 days, fixing with 4% paraformaldehyde every 24 h and mounting coverslips with ProlongGold (Invitrogen). Coverslips were then imaged with a 20x air objective for further analysis using ImageJ (NIH).

Proliferation assay

NIH3T3 and HT1080 cells were seeded in a 96-well plate at 1000 cells per well and incubated for 4 h. Growth medium was then carefully removed and 1X CyQUANT® NF (Invitrogen) dye reagent was added. Cells were then incubated at 37°C for 1 h. This incubation period is required for equilibration of dye–DNA binding, resulting in a stable fluorescence endpoint. The fluorescence intensity of each sample was then imaged every 24 h using a fluorescence microplate reader with excitation at ~485 nm and emission detection at ~530 nm. Fresh growth medium was added every 48 h. Cell numbers at each time-point were determined using a standard curve as per the manufacturer's instructions.

Statistical analyses

Statistical analyses are described in each figure legend.

REFERENCES

ABERCROMBIE, M. 1979. Contact inhibition and malignancy. *Nature,* 281**,** 259-62.

AOKI, K., KONDO, Y., NAOKI, H., HIRATSUKA, T., ITOH, R. E. & MATSUDA, M. 2017. Propagating Wave of ERK Activation Orients Collective Cell Migration. *Dev Cell,* 43**,** 305-317 e5.

AOKI, K. & MATSUDA, M. 2009. Visualization of small GTPase activity with fluorescence resonance energy transfer-based biosensors. *Nat Protoc,* 4**,** 1623-31.

ARAGONA, M., PANCIERA, T., MANFRIN, A., GIULITTI, S., MICHIELIN, F., ELVASSORE, N., DUPONT, S. & PICCOLO, S. 2013. A mechanical checkpoint controls multicellular growth through YAP/TAZ regulation by actin-processing factors. *Cell,* 154**,** 1047-1059.

BETZ, T., KOCH, D., LIM, D. & KAS, J. A. 2009. Stochastic actin polymerization and steady retrograde flow determine growth cone advancement. *Biophys J,* 96**,** 5130-8.

DAVIS, J. R., HUANG, C. Y., ZANET, J., HARRISON, S., ROSTEN, E., COX, S., SOONG, D. Y., DUNN, G. A. & STRAMER, B. M. 2012. Emergence of embryonic pattern through contact inhibition of locomotion. *Development,* 139**,** 4555-60.

DAVIS, J. R., LUCHICI, A., MOSIS, F., THACKERY, J., SALAZAR, J. A., MAO, Y., DUNN, G. A., BETZ, T., MIODOWNIK, M. & STRAMER, B. M. 2015. Inter-cellular forces orchestrate contact inhibition of locomotion. *Cell,* 161**,** 361-73.

DUNN, G. A. & PADDOCK, S. W. 1982. Analysing the motile behaviour of cells: a general approach with special reference to pairs of cells in collision. *Philos Trans R Soc Lond B Biol Sci,* 299**,** 147-57.

ELOWE, S., HOLLAND, S. J., KULKARNI, S. & PAWSON, T. 2001. Downregulation of the Ras-mitogen-activated protein kinase pathway by the EphB2 receptor tyrosine kinase is required for ephrin-induced neurite retraction. *Mol Cell Biol,* 21**,** 7429-41.

FOTY, R. A. & STEINBERG, M. S. 2013. Differential adhesion in model systems. *Wiley Interdiscip Rev Dev Biol,* 2**,** 631-45.

GUMBINER, B. M. & KIM, N. G. 2014. The Hippo-YAP signaling pathway and contact inhibition of growth. *J Cell Sci,* 127**,** 709-17.

HOCKEL, M. 2012. Cancer permeates locally within ontogenetic compartments: clinical evidence and implications for cancer surgery. *Future Oncol,* 8**,** 29-36.

HOCKEL, M. 2015. Morphogenetic fields of embryonic development in locoregional cancer spread. *Lancet Oncol,* 16**,** e148-51.

KANDOUZ, M., HAIDARA, K., ZHAO, J., BRISSON, M. L. & BATIST, G. 2010. The EphB2 tumor suppressor induces autophagic cell death via concomitant activation of the ERK1/2 and PI3K pathways. *Cell Cycle,* 9**,** 398-407.

KOMATSU, N., AOKI, K., YAMADA, M., YUKINAGA, H., FUJITA, Y., KAMIOKA, Y. & MATSUDA, M. 2011. Development of an optimized backbone of FRET biosensors for kinases and GTPases. *Mol Biol Cell,* 22**,** 4647-56.

MENDOZA, M. C., ER, E. E., ZHANG, W., BALLIF, B. A., ELLIOTT, H. L., DANUSER, G. & BLENIS, J. 2011. ERK-MAPK drives lamellipodia protrusion by activating the WAVE2 regulatory complex. *Mol Cell,* 41**,** 661-71.

MIAO, H., NICKEL, C. H., CANTLEY, L. G., BRUGGEMAN, L. A., BENNARDO, L. N. & WANG, B. 2003. EphA kinase activation regulates HGF-induced epithelial branching morphogenesis. *J Cell Biol,* 162**,** 1281-92.

PAWLIZAK, S., FRITSCH, A. W., GROSSER, S., AHRENS, D., THALHEIM, T., RIEDEL, S., KIEßLING, T. R., OSWALD, L., ZINK, M., MANNING, M. L. & KÄS, J. A. 2015. Testing the differential adhesion hypothesis across the epithelial−mesenchymal transition. *New J Phys,* 17, 083049.

POLIAKOV, A., COTRINA, M. L., PASINI, A. & WILKINSON, D. G. 2008. Regulation of EphB2 activation and cell repulsion by feedback control of the MAPK pathway. *J Cell Biol,* 183**,** 933-47.

PORAZINSKI, S., DE NAVASCUES, J., YAKO, Y., HILL, W., JONES, M. R., MADDISON, R., FUJITA, Y. & HOGAN, C. 2016. EphA2 Drives the Segregation of Ras-Transformed Epithelial Cells from Normal Neighbors. *Curr Biol,* 26**,** 3220-3229.

PRATT, R. L. & KINCH, M. S. 2002. Activation of the EphA2 tyrosine kinase stimulates the MAP/ERK kinase signaling cascade. *Oncogene,* 21**,** 7690-9.

SADATI, M., TAHERI QAZVINI, N., KRISHNAN, R., PARK, C. Y. & FREDBERG, J. J. 2013. Collective migration and cell jamming. *Differentiation,* 86**,** 121-5.

STRAMER, B. & MAYOR, R. 2016. Mechanisms and in vivo functions of contact inhibition of locomotion. *Nat Rev Mol Cell Biol*.

TAMBE, D. T. & FREDBERG, J. J. 2015. And I hope you like jamming too. *New J Phys,* 17, 091001.

THEVENEAU, E., STEVENTON, B., SCARPA, E., GARCIA, S., TREPAT, X., STREIT, A. & MAYOR, R. 2013. Chase-and-run between adjacent cell populations promotes directional collective migration. *Nat Cell Biol,* 15**,** 763-72.

VINDIS, C., CERRETTI, D. P., DANIEL, T. O. & HUYNH-DO, U. 2003. EphB1 recruits c-Src and p52Shc to activate MAPK/ERK and promote chemotaxis. *J Cell Biol,* 162**,** 661-71.

YANG, J. M., BHATTACHARYA, S., WEST-FOYLE, H., HUNG, C. F., WU, T. C., IGLESIAS, P. A. & HUANG, C. H. 2018. Integrating chemical and mechanical signals through dynamic coupling between cellular protrusions and pulsed ERK activation. *Nat Commun,* 9**,** 4673.

Funding

This project has received funding from the European Research Council (ERC) under the European Union's Horizon 2020 research and innovation program grant agreement No. 681808. T.H. has received funding from the European Union's Horizon 2020 research and innovation program under the Marie Sklodowska-Curie grant agreement No. 704587. F.N.K. and B.M.S. are funded by a Wellcome Trust Investigator Award, grant number WT107859/Z/15/Z. Deposited in PMC for release....

Figure Legends

Fig. 1. Fibroblasts and fibrosarcoma cells exhibit distinct responses upon collision with epithelial cells

(A) Confrontation assay between epithelial cells (HaCaT, green) and fibroblasts (NIH3T3, magenta) or fibrosarcoma cells (HT1080, magenta). Red line indicates collision-point. Scale bars = 100 μm.

(B) HaCaT displacement 24 h after colliding with NIH3T3 or HT1080 cells (n = 3, error bars = SEM, ***P < 0.001).

(C) Leading-edge speed of migrating HaCaT cells when no other cell population is encountered (n = 3, error bars = SEM).

(D) Leading-edge speed of migrating HaCaT cells involving collision with either NIH3T3 or HT1080 cell populations. Dotted line indicates collision-point (n = 3, error bars = SEM).

(E) PIV analysis of the HaCaT and HT1080 interaction in 'A' showing global increase in HaCaT speed despite collision with HT1080 cells. Blue-red represents a shift from low to high velocity.

Fig. 2. Fibrosarcoma cells undergo active repulsion upon collision with epithelial cells which is perturbed by EphB2 or ERK1/2 knockdown

(A) Vectors depicting acceleration changes upon collision (time = 0 min) normalised to the position of the colliding partner (large arrow). A significant rearward acceleration (**P < 0.01, non-parametric Wilcoxon signed-rank test) is only observed in HT1080 vs HaCaT collision (n ≥ 6 collisions).

(B) Vectors depicting velocity of colliding cells before, at time of, and after collision normalised to the position of the colliding partner (large arrow). A significant post-collision rearward velocity away from the colliding partner (*P < 0.05, non-parametric Wilcoxon signed-rank test) is only observed in HT1080 vs HaCaT (n ≥ 6 collisions).

(C) Cell distance from colliding partner during heterotypic and homotypic collisions between HT1080, NIH3T3, and HaCaT cells. Following collision (dotted line), only HT1080 and HaCaT cells rapidly separate (n ≥ 6 collisions, error bars = SEM).

(D) Cell distance from colliding partner during heterotypic HaCaT-HT1080 collisions comparing non-transfected (HaCaT vs HT1080 from 'C') with EphB2 or ERK1/2 knockdown (HT1080) (n ≥ 6 collisions, error bars = SEM).

(E) Time taken for HT1080 cells to retract their leading-edge following contact with HaCaT cells (n ≥ 7 collisions per condition, line = mean, error bars ± SD, *P < 0.05, **P < 0.01, Student's t-test).

(F) Time between leading-edge retraction and formation of a protrusion in HT1080 cells following contact with HaCaT cells. Negative values indicate that formation of the new protrusion occurred *before* leading-edge retraction (n ≥ 7 collisions, line = mean, error bars ± SD, **P < 0.01, ****P < 0.0001, Student's t-test).

Fig. 3. ERK activation is elevated in collisions between epithelial and fibrosarcoma cells

(A) Western blot reveals pERK was highest during co-culture of HaCaT and HT1080 cells. (n = 3, error bars = SEM).

(B) Western blot and quantification showing total ERK was unaffected by EphB2 knockdown in HT1080 cells compared with non-transfected control. (n = 3, error bars = SEM, ns = not statistically significant, Student's t-test).

(C) Western blot and quantification showing pERK was significantly reduced in the co-culture after EphB2 knockdown in HT1080 cells compared with non-transfected control. (n = 3, error bars = SEM, **P < 0.01, Student's t-test).

(D) Confrontation assay between HaCaT cells (unlabelled) and HT1080 cells expressing the ERK FRET-biosensor. Scale bar = 50 μm.

(E) ERK activity in the leading row of HT1080 cells in the confrontation assay before collision, after collision and in rear cells after collision. (n = 29 cells per condition, boxplots represent range, median and quartiles, *P < 0.05, ***P < 0.001 Mann-Whitney test).

(F) ERK activity in the leading row of NIH3T3 cells in the confrontation assay before and after collision (n = 23 cells per condition, boxplots represent range, median and quartiles, ns = not statistically significant, Mann-Whitney test).

(G) ERK activity from four representative tracks of HT1080 cells cultured alone (blue) or co-cultured with HaCaT cells (red).

(H) Fluctuation of ERK activity as measured by variance in randomly selected tracks

of HT1080 cells cultured alone or co-cultured with HaCaT cells. (n = 15 tracks, line = mean, error bars ± SD, ***P < 0.001, Mann-Whitney test).

Fig. 4. Fibrosarcoma cells sort from epithelial cells in culture, a behaviour which is disrupted by EphB2 or ERK1/2 knockdown

(A) Screenshots from movies of co-cultures of epithelial cells (HaCaT, green) with either fibroblasts (NIH3T3, magenta) or fibrosarcoma cells (HT1080, magenta). Scale bar = 100 μm.

(B) Tracks of NIH3T3 or HT1080 cells throughout the movies in 'A'.

(C) Images (fixed after 24 h) of HaCaT cells (green) co-cultured with Control, EphB2 or ERK1/2 siRNA transfected HT1080 cells (magenta). Scale Bar = 100 μm.

(D) Dispersion of HaCaT cells in 'C' quantified by measuring their distribution of nearest-neighbour distances. (n = 3, error bars = SEM, **P < 0.01, *P < 0.05, Student's t-test).

(E) Long term culture of HaCaT cells (green) alone or co-cultured with NIH3T3 or HT1080 cells (unlabeled). Scale bar = 100 μm.

(F) HaCaT cell-number when grown in isolation or co-cultured showing reduced HaCaT proliferation when co-cultured with NIH3T3 cells but not HT1080 cells.

(G) Size of individual HaCaT cells showing reduced spreading when contacting NIH3T3 cells but not HT1080 cells. (****P < 0.0001, ns = not statistically significant, Mann-Whitney test, n ≥ 69 cells per condition).

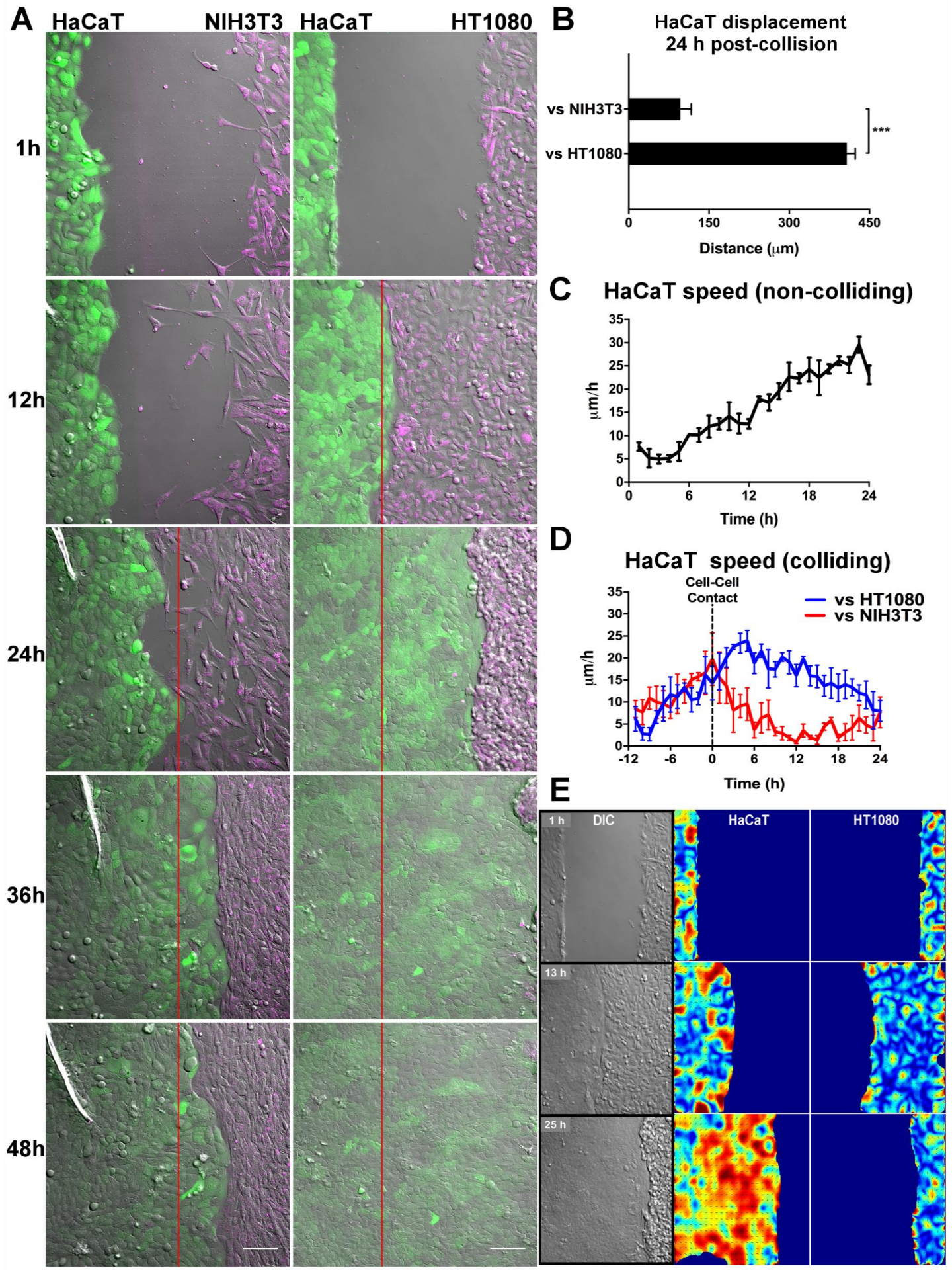
A
HaCaT
NIH3T3
HaCaT
HT1080
1h
12h
24h
36h
48h
B
HaCaT displacement
24 h post-collision
vs NIH3T3
vs HT1080
***
0
150
300
450
Distance (μm)
C
HaCaT speed (non-colliding)
μm/h
0
5
10
15
20
25
30
35
0
6
12
18
24
Time (h)
D
HaCaT speed (colliding)
Cell-Cell
Contact
vs HT1080
vs NIH3T3
μm/h
-12
-6
0
6
12
18
24
Time (h)
E
1 h
DIC
HaCaT
HT1080
13 h
25 h

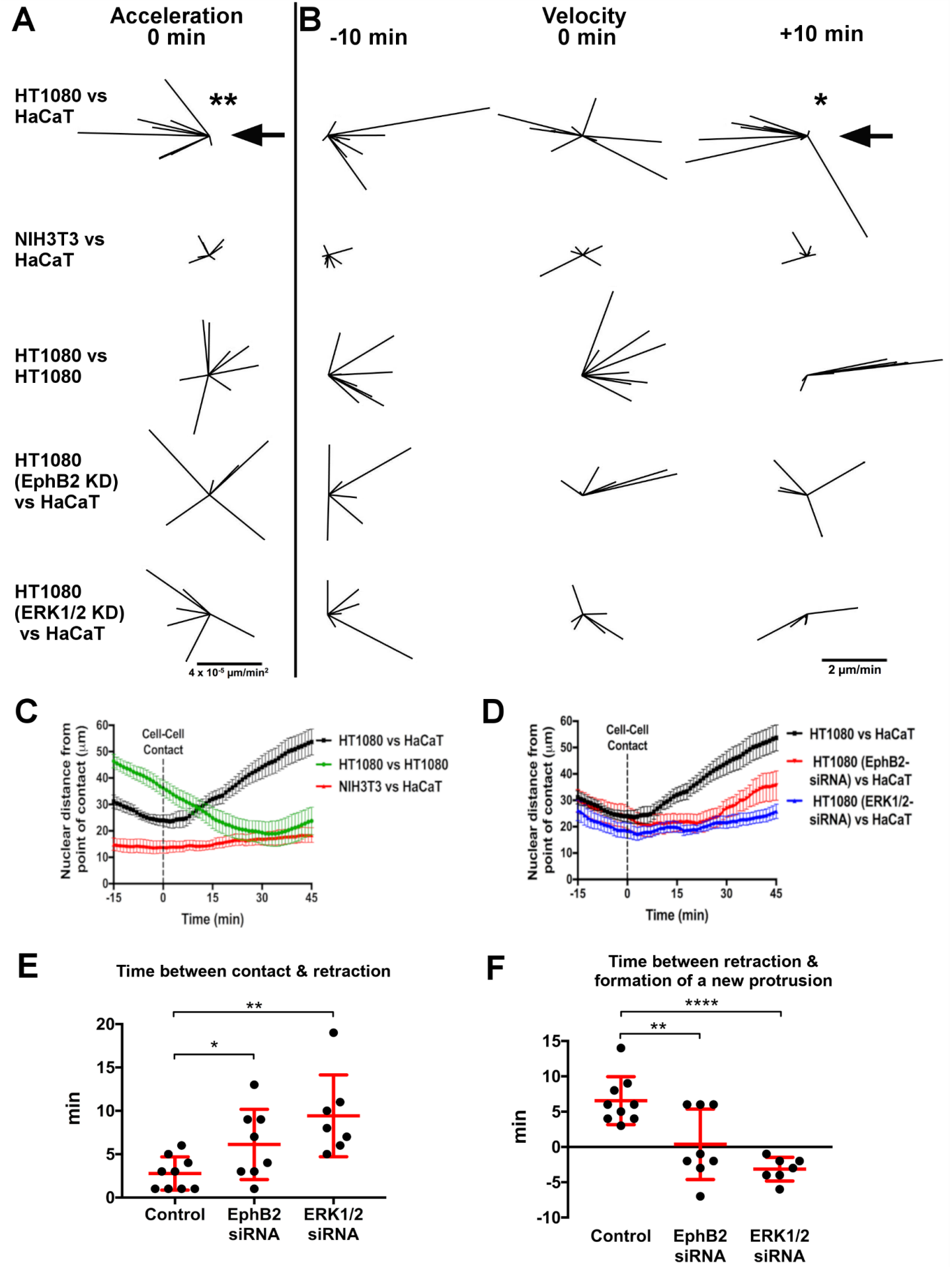
A
Acceleration
0 min
B
-10 min
Velocity
0 min
+10 min
HT1080 vs HaCaT
NIH3T3 vs HaCaT
HT1080 vs HT1080
HT1080 (EphB2 KD) vs HaCaT
HT1080 (ERK1/2 KD) vs HaCaT
**
*
4 x 10-5 µm/min2
2 µm/min
C
Cell-Cell Contact
Nuclear distance from point of contact (µm)
Time (min)
HT1080 vs HaCaT
HT1080 vs HT1080
NIH3T3 vs HaCaT
D
Cell-Cell Contact
Nuclear distance from point of contact (µm)
Time (min)
HT1080 vs HaCaT
HT1080 (EphB2-siRNA) vs HaCaT
HT1080 (ERK1/2-siRNA) vs HaCaT
E
Time between contact & retraction
min
**
*
Control
EphB2 siRNA
ERK1/2 siRNA
F
Time between retraction & formation of a new protrusion
min
****
**
Control
EphB2 siRNA
ERK1/2 siRNA

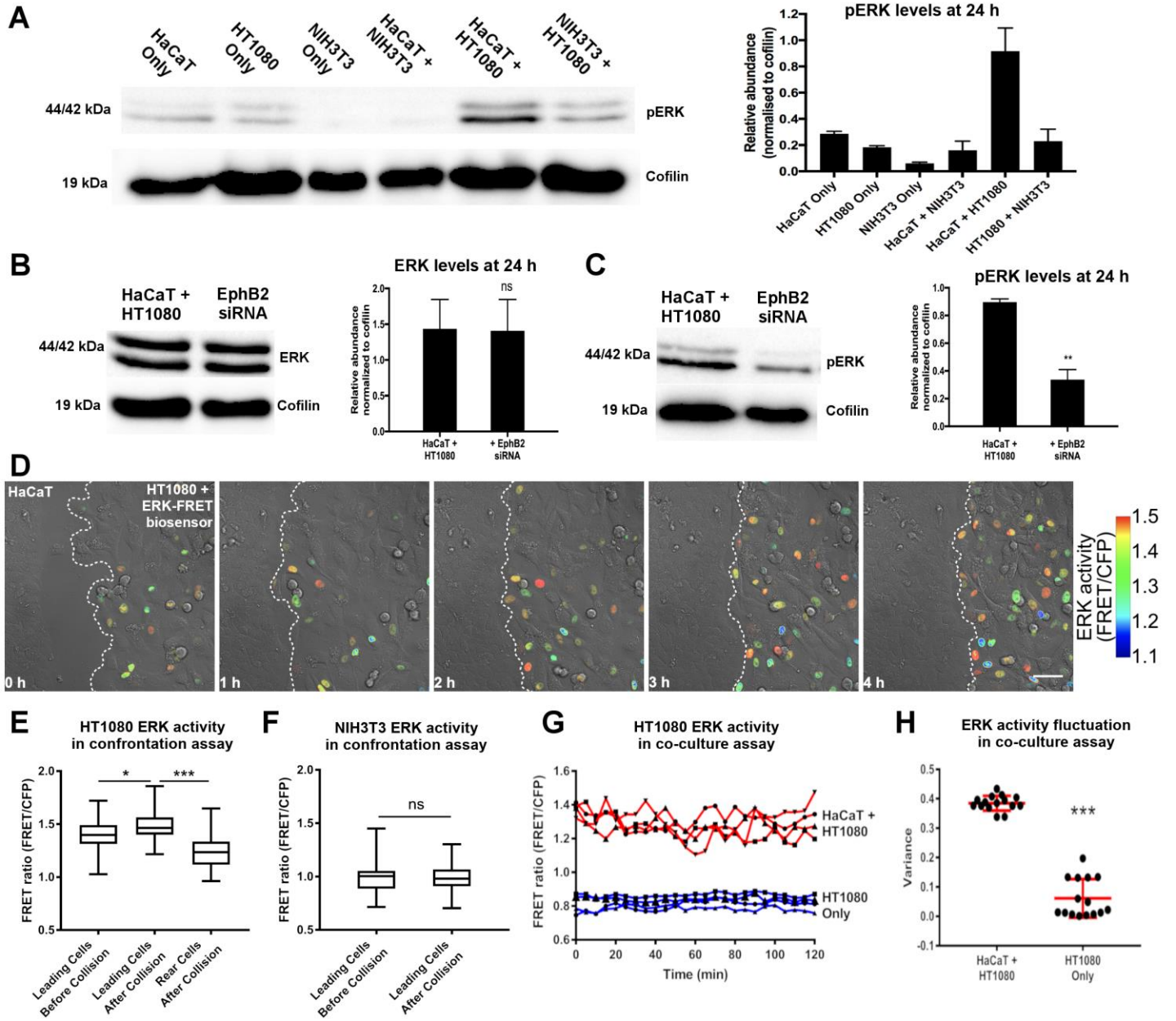
A
HaCaT Only
HT1080 Only
NIH3T3 Only
HaCaT + NIH3T3
HaCaT + HT1080
NIH3T3 + HT1080
44/42 kDa
pERK
19 kDa
Cofilin
pERK levels at 24 h
Relative abundance (normalised to cofilin)
HaCaT Only
HT1080 Only
NIH3T3 Only
HaCaT + NIH3T3
HaCaT + HT1080
HT1080 + NIH3T3
B
HaCaT + HT1080
EphB2 siRNA
44/42 kDa
ERK
19 kDa
Cofilin
ERK levels at 24 h
ns
Relative abundance normalized to cofilin
HaCaT + HT1080
+ EphB2 siRNA
C
HaCaT + HT1080
EphB2 siRNA
44/42 kDa
pERK
19 kDa
Cofilin
pERK levels at 24 h
**
Relative abundance normalized to cofilin
HaCaT + HT1080
+ EphB2 siRNA
D
HaCaT
HT1080 + ERK-FRET biosensor
0 h
1 h
2 h
3 h
4 h
ERK activity (FRET/CFP)
1.5
1.4
1.3
1.2
1.1
E
HT1080 ERK activity in confrontation assay
FRET ratio (FRET/CFP)
*
***
Leading Cells Before Collision
Leading Cells After Collision
Rear Cells After Collision
F
NIH3T3 ERK activity in confrontation assay
FRET ratio (FRET/CFP)
ns
Leading Cells Before Collision
Leading Cells After Collision
G
HT1080 ERK activity in co-culture assay
FRET ratio (FRET/CFP)
HaCaT + HT1080
HT1080 Only
Time (min)
H
ERK activity fluctuation in co-culture assay
Variance
***
HaCaT + HT1080
HT1080 Only

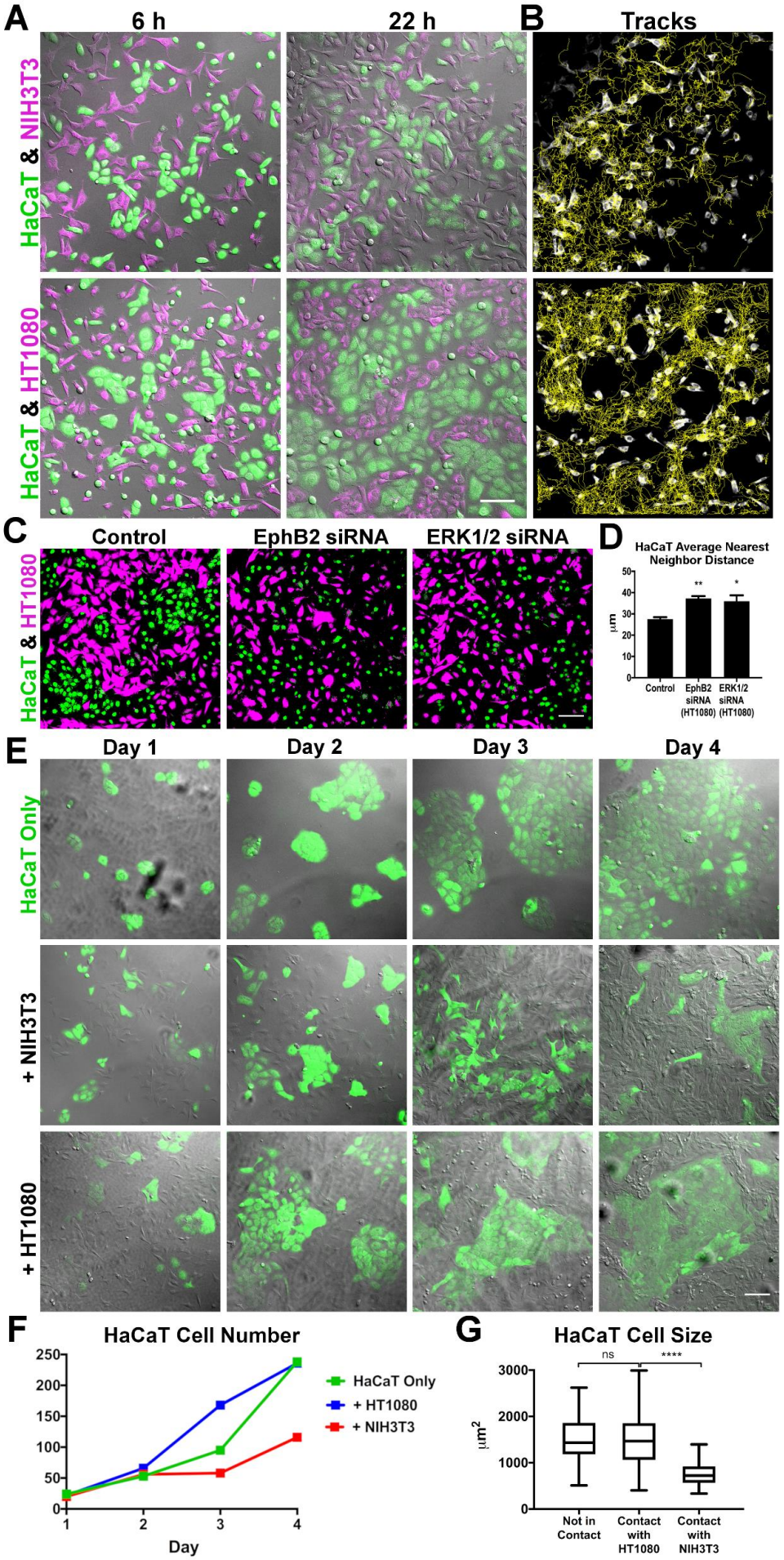
A
6 h
22 h
B
Tracks
HaCaT & NIH3T3
HaCaT & HT1080
C
Control
EphB2 siRNA
ERK1/2 siRNA
HaCaT & HT1080
D
HaCaT Average Nearest Neighbor Distance
µm
50
40
30
20
10
0
**
*
Control
EphB2 siRNA (HT1080)
ERK1/2 siRNA (HT1080)
E
Day 1
Day 2
Day 3
Day 4
HaCaT Only
+ NIH3T3
+ HT1080
F
HaCaT Cell Number
250
200
150
100
50
0
1
2
3
4
Day
HaCaT Only
+ HT1080
+ NIH3T3
G
HaCaT Cell Size
ns
****
µm2
3000
2000
1000
0
Not in Contact
Contact with HT1080
Contact with NIH3T3

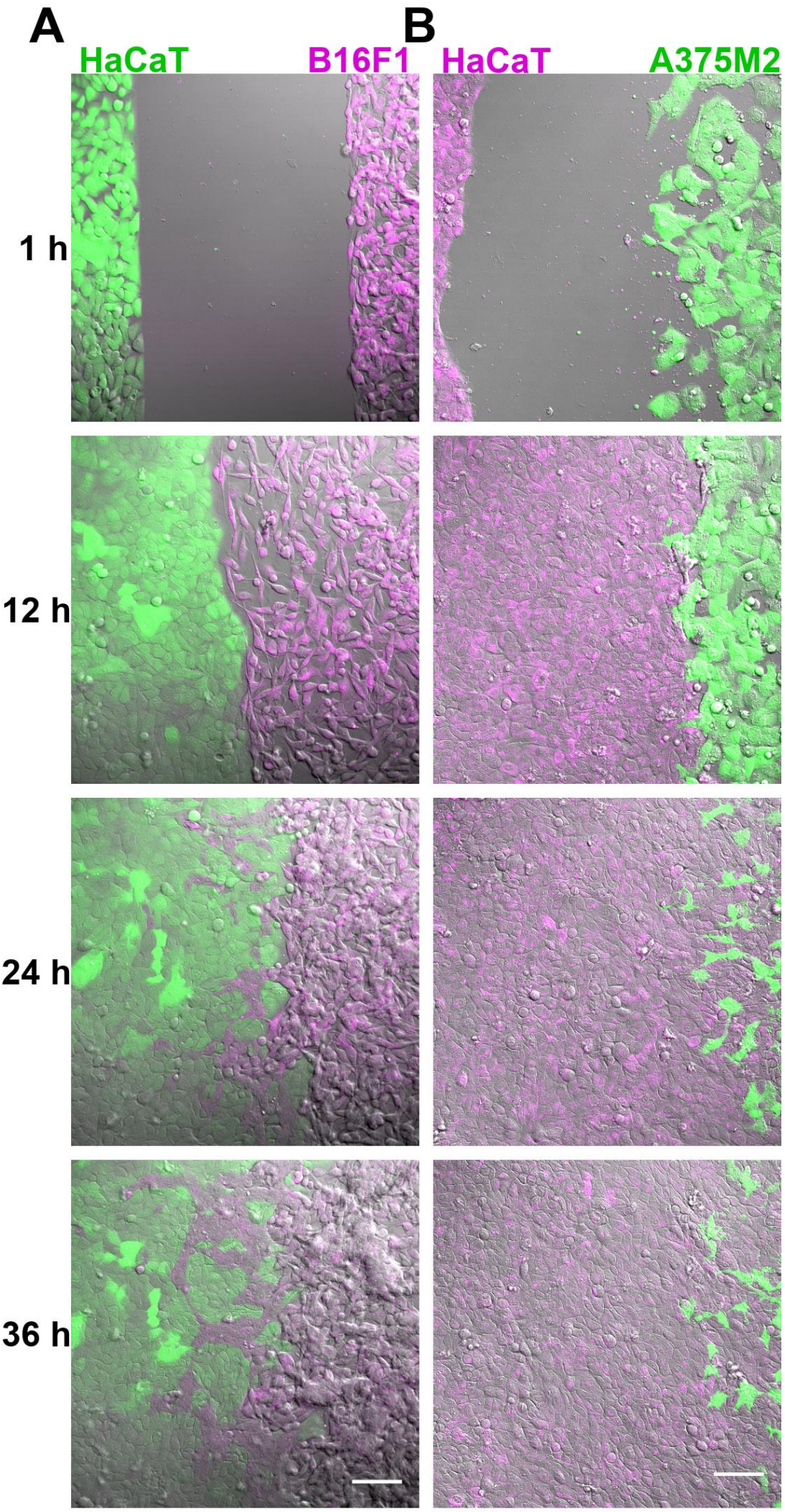

Figure S1.

(A) Confrontation assay between HaCaT human keratinocytes (green) and B16F1 mouse melanoma cells (magenta).
(B) Confrontation assay between HaCaT human keratinocytes (magenta) and A375M2 human melanoma cells (green).
Scale bars = 100 µm.

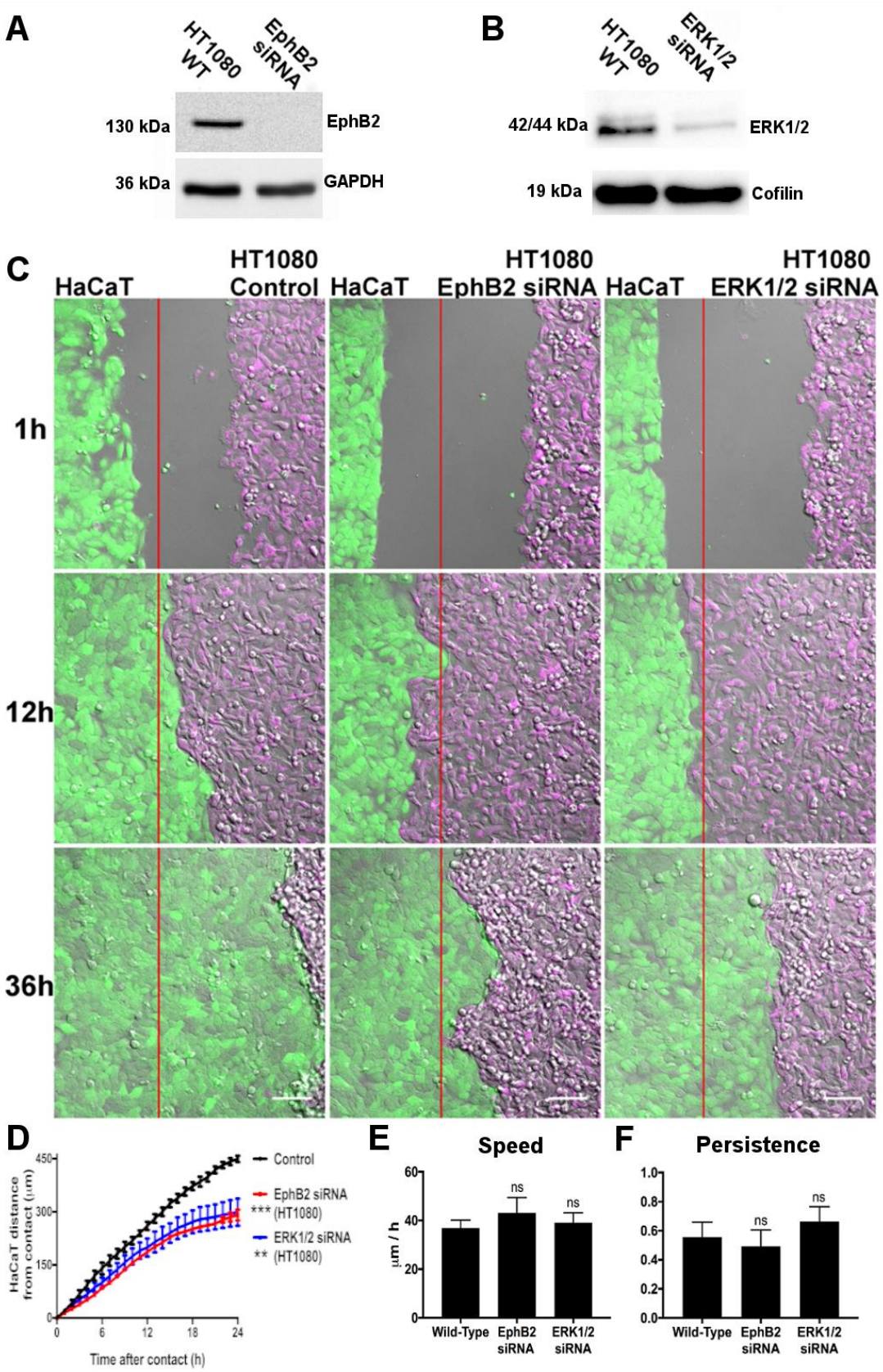

Figure S2.

(A) Western blot confirming knockdown of EphB2 protein in HT1080 cells 48 h post-transfection with siRNA compared with non-transfected cells (WT = Wild Type).

(B) Western blot confirming knockdown of ERK1/2 protein in HT1080 cells 48 h post-transfection with siRNA compared with non-transfected cells (WT = Wild Type).

(C) Screenshots from a confrontation assay in which HaCaT cells (green) are allowed to collide with either Control, EphB2 or ERK1/2 siRNA transfected HT1080 cells (magenta). Red line indicates position of contact. Scale bars = 100 µm.

(D) Displacement of HaCaT leading-edge after collision with HT1080 cells (Control, EphB2 or ERK1/2 siRNA) in the confrontation assay. (n = 3, error bars = SEM, ***P < 0.001, **P < 0.01, Friedman test).

(E) Speed of non-colliding HT1080 cells transfected with either EphB2 or ERK1/2 siRNA compared with non-transfected (wild-type). (n = 10 cells, error bars = SEM, ns = not statistically significant, Student's t-test).

(F) Persistence of non-colliding HT1080 cells transfected with either EphB2 or ERK1/2 siRNA compared with non-transfected (wild-type). (n = 10 cells, error bars = SEM, ns = not statistically significant, Student's t-test).

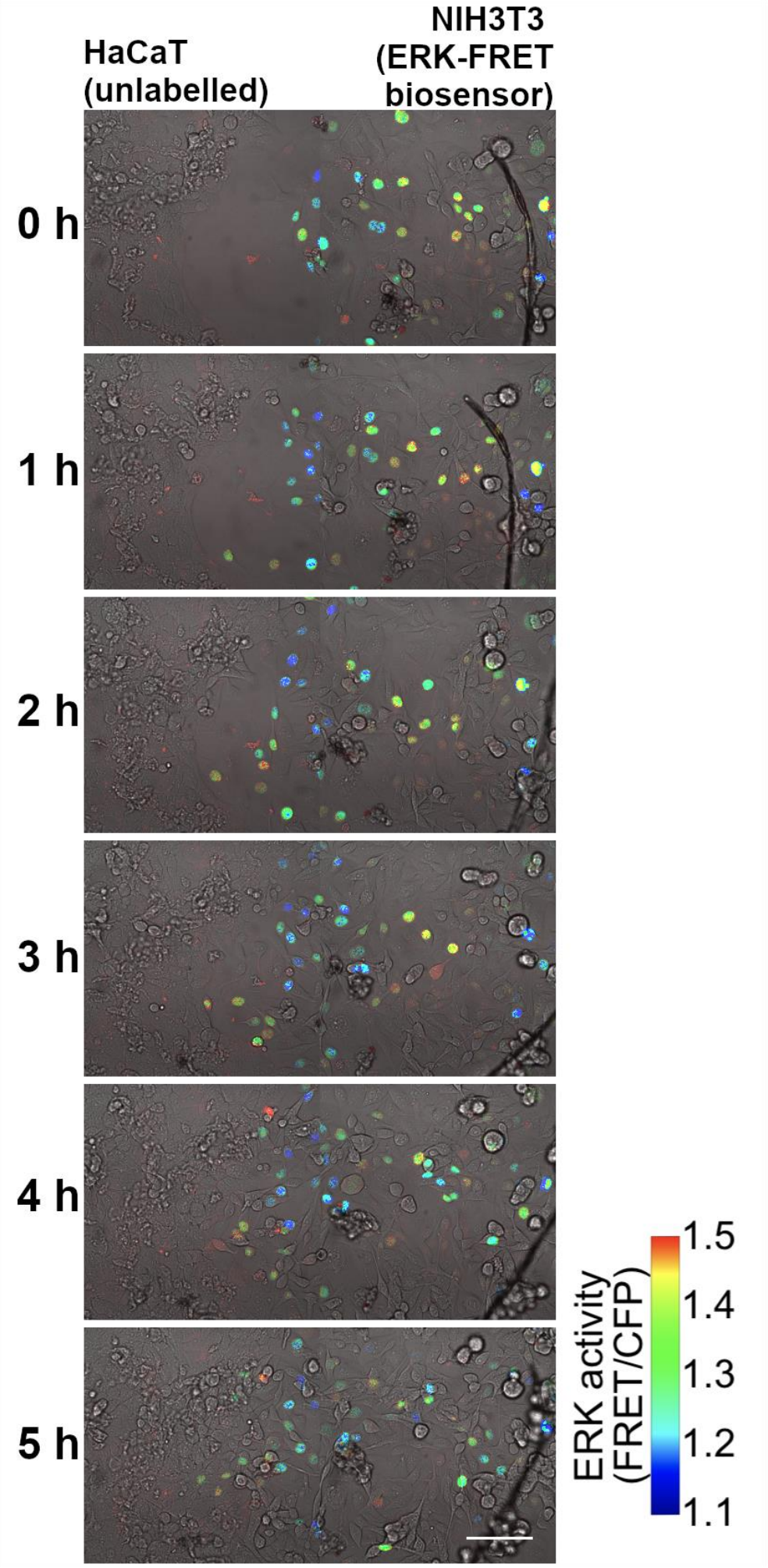

Figure S3. Confrontation assay between HaCaT cells (unlabelled) and NIH3T3 cells expressing the ERK FRET-biosensor. Scale bar = 100 µm.

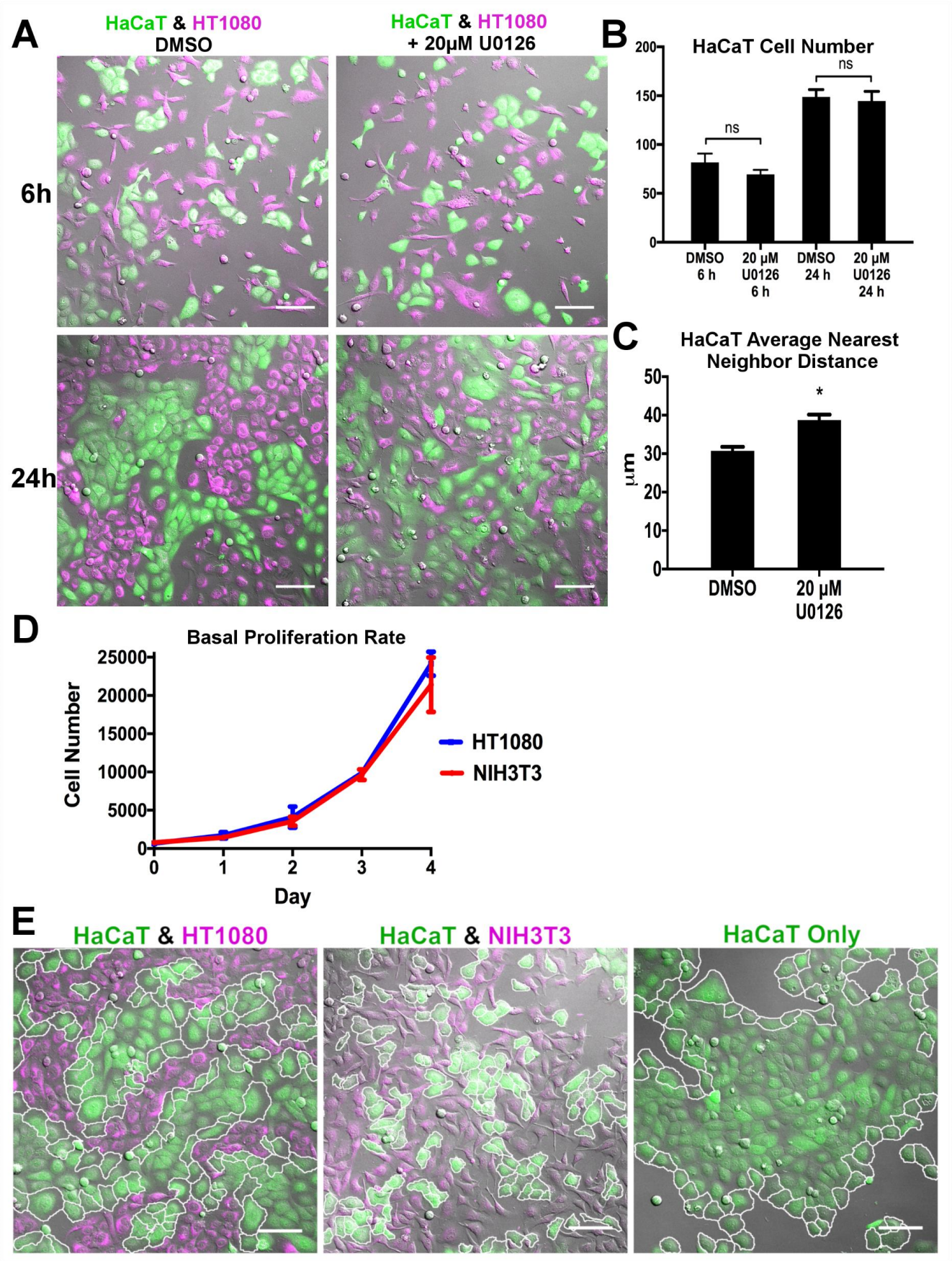

Figure S4.

(A) Images of co-cultures of epithelial cells (HaCaT, green) with fibrosarcoma cells (HT1080, magenta) comparing DMSO vehicle control with 20 μM U0126 treatment to inhibit ERK signalling.

(B) Quantification of HaCaT cell numbers at 6 and 24 h to demonstrate that U0126 does not selectively impact the growth rate of HaCaT cells. (n = 3, error bars = SEM, ns = not statistically significant, Student's t-test).

(C) The dispersion of HaCaT cells at 24 h quantified by measuring their distribution of nearest neighbor distances. An increase in HaCaT dispersion represents a reduction in their segregation from HT1080 cells. (n = 3, error bars = SEM, *P < 0.05, Student's t-test).

(D) Basal proliferation rates of NIH3T3 and HT1080 cells (n = 3, error bars = mean ± SD).

(E) Screenshots showing the extent of spreading (quantified in Fig. 4G) of epithelial cells (outlined in white) when contacting HT1080 cells (left), NIH3T3 cells (middle), and when not in contact with either mesenchymal cell population (cultured alone, right).

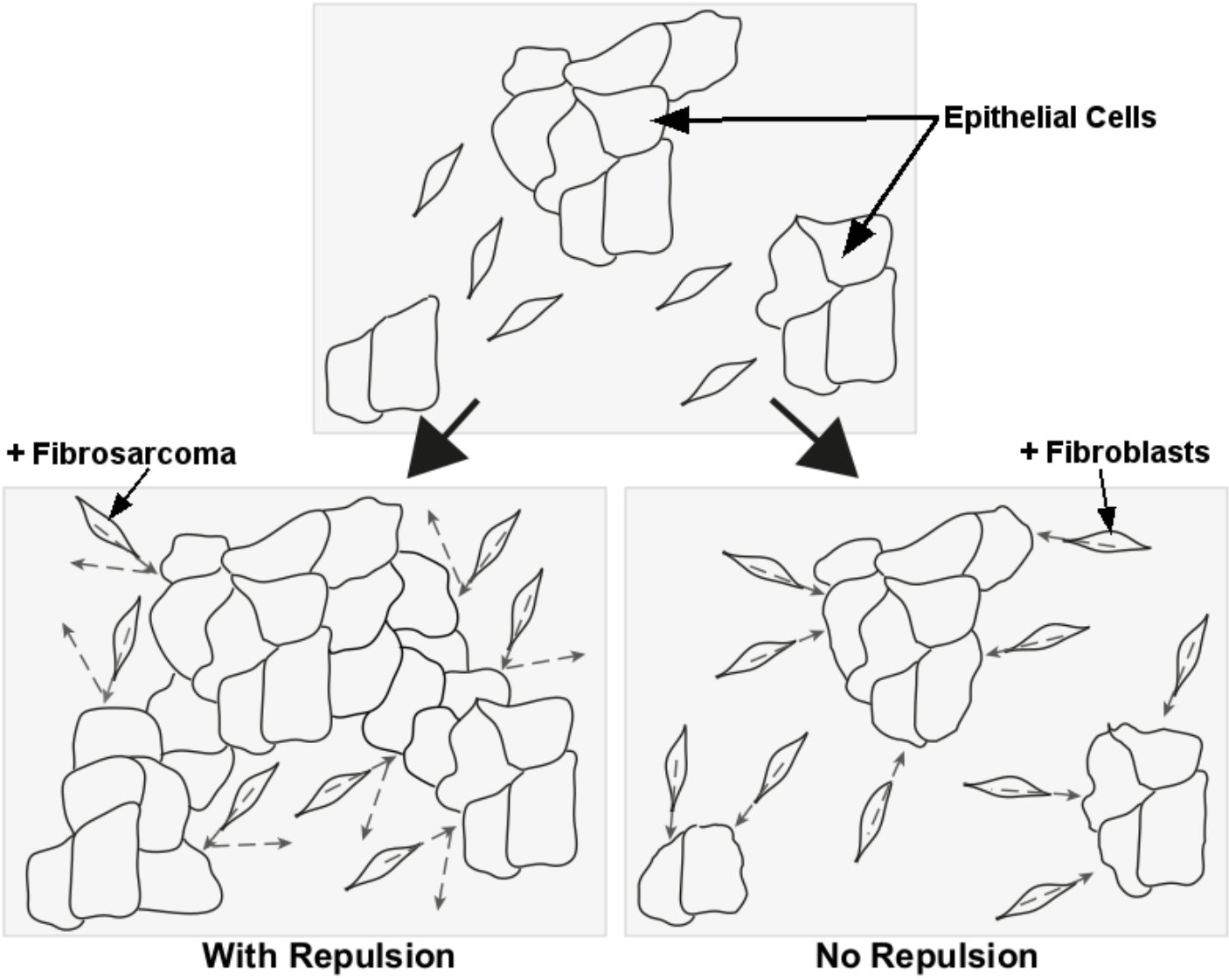

Figure S5. Schematic depicting our model of cell-sorting whereby a mesenchymal cell-type (fibrosarcoma, left) can rapidly and almost completely segregate from an epithelial population. We hypothesise that the strong heterotypic repulsion between fibrosarcoma and epithelial cells allows the epithelial cells to spread. Furthermore, there appears to be an aspect of fibrosarcoma CIL relieving contact inhibition of proliferation of epithelial cells, allowing epithelial colonies to proliferate and merge. In the fibroblast-epithelial combination (right), the epithelial cells are inhibited in their ability to spread due to a lack of heterotypic repulsion, which would enhance the spatial constraint on the epithelial colonies leading to their reduced proliferation. In this case the lack of repulsive CIL prevents the epithelial colonies from growing enough to merge with neighbouring colonies and thus separate from the fibroblast population.

Supplementary Movie Legends

Movie 1.

Confrontation assays between HaCaT epithelial cells (green) and NIH3T3 fibroblasts or HT1080 fibrosarcoma cells (magenta). 1h frames. Scale bar = 100 μm.

Movie 2.

Confrontation assays between:
HaCaT (human keratinocyte, green) vs B16F1 (mouse melanoma, magenta).
HaCaT (human keratinocyte, magenta) vs A375M2 (human melanoma, green).
1 h frames. Scale bar = 100 μm.

Movie 3.

Particle Image Velocimetry (PIV) heat-map of the HaCaT and HT1080 interaction showing global increase in HaCaT cell speed after colliding with HT1080 cells. Blue to red represents a shift from low to high instantaneous velocity.
1 h frames.

Movie 4.

Individual HT1080 fibrosarcoma cells (Control, EphB2 or ERK1/2 siRNA transfected) colliding with HaCaT epithelial cells or homotypic collisions between HT1080 cells. Red lines represent manual tracking used for the kinematics analysis.
10 sec frames. Scale Bar = 20 μm.

Movie 5.

Confrontation assay between HaCaT cells (unlabelled) and HT1080 cells expressing the ERK FRET-biosensor. Blue to red represents an increase in ERK activity (FRET/CFP).
5 min frames. Scale bar = 50 μm.

Movie 6.

(Top) Co-culture assay whereby HaCaT cells (green) are co-cultured with either NIH3T3 cells (left, magenta) or HT1080 cells (right, magenta). 10 min frames. Scale bar = 100 μm.
(Bottom) Tracks of NIH3T3 fibroblasts (left) and HT1080 fibrosarcoma cells (right) from the movies above. Tracks shift blue to red throughout movie to demonstrate that, in the HT1080 case (bottom right), cells become segregated from HaCaT cells (not labelled) over time.